

Fabrication and characterization of a condenser zone plate for compact x-ray microscopy

Stefan Rehbein,^{a)} Anders Holmberg,^{b)} Göran A. Johansson, Per A. C. Jansson, and Hans M. Hertz

Biomedical and X-Ray Physics, Royal Institute of Technology/Albanova, SE-10691 Stockholm, Sweden

(Received 3 September 2003; accepted 14 March 2004; published 24 May 2004)

We describe the in-house fabrication and characterization of a condenser zone plate for a compact laser-plasma-based soft x-ray microscope operating at 2.478 nm wavelength. The fabricated condenser has a diameter of 4.53 mm and an outermost zone width of 49 nm. The pattern is generated by a small-write-field e-beam lithography system and 656 single, 100 μm wide write fields are stitched together to obtain the whole pattern. An in-house method based on a laser-plasma source was developed to characterize the condenser zone plate with regards to diffraction efficiency and imaging properties. The measured groove efficiency of the fabricated condenser zone plate was determined to $11\% \pm 2\%$ and the imaging properties were found to follow the expectations concerning the object field illumination purpose in the x-ray microscope. The in-house characterization method allows faster process improvement in the small-scale laboratory compared to presently used synchrotron-based methods. © 2004 American Vacuum Society. [DOI: 10.1116/1.1738671]

I. INTRODUCTION

Soft x-ray microscopy in the water-window region ($\lambda = 2.3\text{--}4.4$ nm) is an attractive technique for high-resolution (~ 30 nm) imaging¹ of, e.g., biological samples in their aqueous environment. Unfortunately, all operational x-ray microscopes are based on synchrotron radiation sources, which limit their accessibility. Many biological investigators would benefit from having the x-ray microscope in their own laboratory. For this purpose we recently demonstrated a compact x-ray microscope with subvisible resolution operating with an ethanol-liquid-jet laser-plasma source providing $\lambda = 3.37$ nm radiation.² The compact full-field microscope is based on a normal-incidence multilayer condenser optic with an average reflectivity of $\sim 0.5\%$ and a diffractive zone plate objective. A reduction of the operating wavelength to, e.g., 2.478 nm would be advantageous since this wavelength exhibits a significantly lower absorption in water and carbon-based substances, making imaging of thicker samples or samples in aqueous environment less difficult compared to $\lambda = 3.37$ nm. Another advantage of using $\lambda = 2.478$ nm is the possibility to use a liquid-nitrogen-jet laser-plasma instead of an ethanol jet to generate the x rays.³ The nitrogen plasma source produces no carbon debris and therefore causes no long-term degradation of the condenser optic by carbon contamination.

At present there are no multilayer condenser optics available which are suited for our microscope at a wavelength of 2.478 nm. This is due to the difficulty of the fabrication process and so far there are only a few initial results indicating the feasibility of such multilayer mirrors in the future.⁴ Alternatively, the condenser-zone-plate arrangement used in synchrotron-based microscopes may be employed. The

fabrication of such zone plates have relied either on holographic methods⁵ or e-beam lithography.^{6,7} In the latter case, e-beam lithography systems with large write fields have been used. The diffraction-efficiency characterization has typically been performed at synchrotron radiation laboratories.

In the present article we also demonstrate that e-beam systems with small write field are suitable for writing large-diameter condenser zone plates (CZPs) for compact x-ray microscopy. Furthermore, it is shown that in-house characterization of the fabricated CZP can be performed with a laser-plasma source, both with regards to the local diffraction efficiency and the imaging properties. We report 11% diffraction efficiency and conclude that the imaging properties follow the assumption that the significant stitching errors of the e-beam system only have a negligible influence on the image size of the incoherent laser-plasma source. This laser-plasma method is the first compact tool for the characterization of a CZP. It should be noted that the possibility to have both fabrication and characterization facilities in-house leads to faster turnaround time and, thus, improved fabrication of these devices.

II. ZONE PLATE CONDENSER

Figure 1 shows the general arrangement of an x-ray microscope using a CZP. The CZP was designed to image the $\lambda = 2.478$ nm liquid-nitrogen-jet target laser-plasma x-ray source with a magnification of 1 onto the sample. The source has a diameter of ~ 20 μm full width half maximum (FWHM). In front of the CZP an opaque central stop (CS) is mounted, in order to generate a hollow-cone illumination, which determines the usable image field size in the x-ray microscope. The CZP in combination with the CS and a pinhole in the sample plane represent a zone plate

^{a)}Present address: BESSY GmbH, Albert-Einstein-Straße 15, D-12489 Berlin, Germany; electronic mail: rehbein@bessy.de

^{b)}Electronic mail: anders.holmberg@bio.kth.se

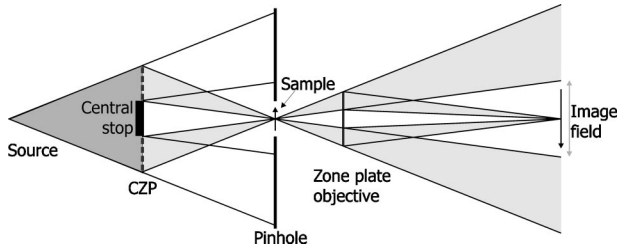


FIG. 1. Arrangement for a compact x-ray microscope employing a condenser zone plate (CZP). The light gray color illustrates the path of the x rays passing the CZP and are diffracted in their +first diffraction order.

linear monochromator.⁸ The monochromatically illuminated sample is imaged with high magnification by a micro-zone-plate objective in the image plane.

The CZP will be used in the +first diffraction order and has the following parameters. The diameter is 4.53 mm and the diameter of the CS is 3.778 mm, i.e., only a $\sim 400 \mu\text{m}$ wide CZP ring containing zones has to be fabricated. The focal length in the first diffraction order at $\lambda=2.478 \text{ nm}$ wavelength is 90 mm and the zone width ranges from 59 nm wide inner zones to 49 nm wide outermost zones.

For high diffraction efficiency at $\lambda=2.478 \text{ nm}$ a nickel zone height of 200 nm was manufactured. The optimal zone height can be calculated following Ref. 9. The nanostructuring process is based on electron-beam lithography, reactive ion etching (RIE), and electroplating of nickel.

The e-beam exposure was performed with a RAITH 150 e-beam lithography system equipped with a laser-interferometer-controlled stage and operated at 30 keV e-beam energy. The only possibility to expose the large CZP pattern with the system is to stitch many small write fields together to obtain the whole pattern. The field stitching leads to an unwanted stitching error between the single fields. The specification of the stitching accuracy of the RAITH 150 e-beam system is 60 nm (3σ). Another effect leading to pattern misplacement during the exposure is a drift of the electron beam, with respect to the sample. This can be caused by thermal and charging effects in the column, stage, chamber, or sample itself. In our system the drift rate is $<2 \text{ nm/min}$. For exposing the CZP pattern a write field size of $100 \mu\text{m} \times 100 \mu\text{m}$ was found to be appropriate concerning resolution, i.e., exposure of $\leq 50 \text{ nm}$ lines, and small intrafield distortion. 656 write fields were stitched together to expose the whole CZP pattern. The circular zones of the CZP were approximated by 10 μm long straight lines. The exposure of the CZP pattern took about 17 h at a probe current of 582 pA. No drift correction was done during the exposure, therefore the largest error (maximum 2 μm) in misplacement of a write field is caused by the drift.

The whole fabrication process of the CZP is depicted in Fig. 2. A 150 nm thick Si_3N_4 foil is covered with a layer system of 5 nm Cr, 10 nm Ge, 200 nm of a polymer ARC-XL20 (Brewer Science), 5 nm Ti and 40 nm thick e-beam resist ZEP 7000. The e-beam resist layer is exposed with the zone plate pattern and after development [Fig. 2(a)], the pattern is transferred into an intermediate Ti mask by a RIE etch

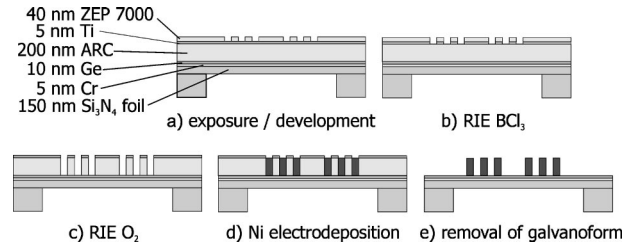


FIG. 2. Process steps for fabricating a nickel CZP.

process with BCl_3 [Fig. 2(b)]. The mask is used for generating a polymer galvanof orm by an O_2 RIE step [Fig. 2(c)]. Afterwards the galvanof orm is filled with nickel (200 nm high) by electrodeposition from a nickel sulphamate bath. In this step the Cr and Ge layers serve as a plating base [Fig. 2(d)]. Finally, the Ti mask and the galvanof orm are removed [Fig. 2(e)] by RIE steps with BCl_3 and O_2 , respectively. This process is described in more detail in Ref. 10.

Figure 3 shows two different images of a CZP with 200 nm high nickel zones and an outermost zone width of 49 nm. The small image in the upper left corner shows an overview of the $\sim 400 \mu\text{m}$ wide CZP ring on a $5 \text{ mm} \times 5 \text{ mm}$ Si_3N_4 foil (bright quadratic area in the black area of the image). The large light microscope image [differential interference contrast (DIC)] in Fig. 3, depicts a small part of the condenser ring at higher magnification. The bright single $100 \mu\text{m} \times 100 \mu\text{m}$ large write fields, which were stitched together to form the ring, are clearly visible. In Fig. 4 a scanning electron microscope (SEM) micrograph of four adjacent single write fields of the CZP is shown. The nickel structures with a period of 100 nm as well as the stitching error of the four write fields are clearly visible. One should also notice that the size of the stitching error is not a fixed value; it varies over the CZP pattern.

We now briefly discuss the influence of stitching errors and drift on the imaging properties of the CZP. In the x-ray microscope the CZP images the source ($\sim 20 \mu\text{m}$ diameter, $\lambda=2.478 \text{ nm}$), which has a distance of 180 mm to the CZP,

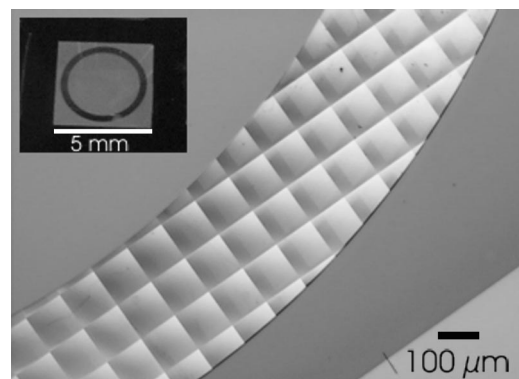


FIG. 3. Small image in the upper left corner shows a photograph of the CZP ring on a $5 \text{ mm} \times 5 \text{ mm}$ Si_3N_4 membrane. The large underlying light microscope image (DIC), shows a small section of the condenser ring on the Si_3N_4 foil.

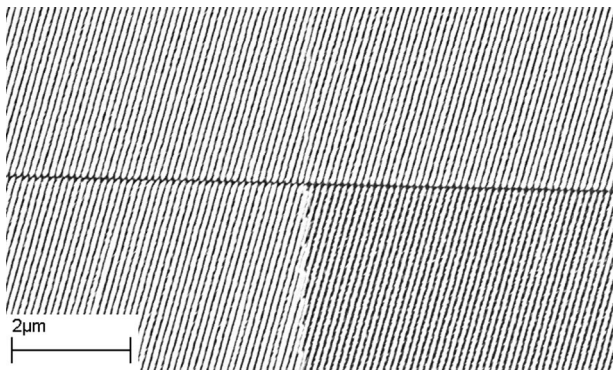


FIG. 4. SEM micrograph shows a section of the Ni zones of the CZP with 100 nm period. The image shows the corners of four adjacent write fields. The field stitching error of the e-beam system is visible.

with a magnification of one into the object plane. Under these conditions, according to the van Cittert–Zernike theorem,¹¹ the spatially coherently illuminated area in the CZP plane is about $7\ \mu\text{m}$ in diameter, which is small compared to a single write field of $100\ \mu\text{m}$ and to the whole CZP diameter. Thus the CZP is, to a good approximation, incoherently illuminated.

Due to the positioning error of the single write fields, the spatial resolution of the e-beam written CZP is significantly lower than given by the Rayleigh criteria $\delta=0.61\lambda/\text{numerical aperture}=1.22\ dr_n/m$ (dr_n is the outermost zone width of the zone plate and m is the diffraction order). Two effects decrease the resolving power: The field stitching error of 60 nm of the e-beam system and the write-field positioning error of up to $2\ \mu\text{m}$ caused by a drift during exposure of the CZP pattern. The field stitching error of 60 nm introduces a phase shift between adjacent fields which redistributes the focused x rays which would be clearly visible under coherent illumination. However, in our case the single write fields are incoherently illuminated. Note that adding up the intensity distributions in the object plane from each source point leads to a much wider distribution of the light than the broadening caused by the field stitching error. The drift during the exposure of the CZP pattern leads to a similar effect, but additionally we have a larger field misplacement of $\leq 2\ \mu\text{m}$. Due to the incoherent illumination we can think of independent write fields, where each single field is imaging the source. A misplacement of a write field will misplace the center of gravity of the corresponding intensity distribution by maximal $2\ \mu\text{m}$ in the image plane. To obtain the source image we superimpose the intensity distributions caused by the single write fields and obtain a slightly broadened source image, compared to a CZP with nonmisplaced write fields. Thus, we conclude that for the illumination purpose of the $20\ \mu\text{m}$ diam object field of the x-ray microscope, the misplacement of the single write fields of the fabricated CZP from their ideal position will not lead to a significant intensity loss and significant intensity variation within the object field compared to the use of an ideal CZP.

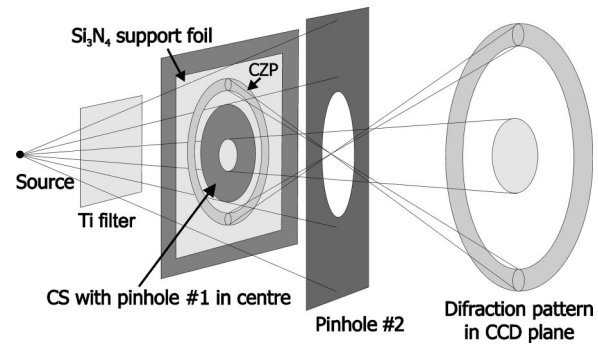


FIG. 5. Experimental arrangement of the efficiency measurement using a laser–plasma source. The diffraction pattern of the CZP and the shadow image of the pinhole in the CS is recorded by a CCD camera.

III. GROOVE EFFICIENCY MEASUREMENTS

Figure 5 depicts the arrangement for the groove efficiency measurements. It is based on a liquid–nitrogen–jet–target laser–plasma source in combination with a 600 nm titanium filter for selecting the NVI emission line at $\lambda=2.88\ \text{nm}$.^{3,12} The typical linewidth is $\lambda/\Delta\lambda\approx 500\text{--}700$ and the filter transmittance may be calculated at Ref. 13. The source illuminates the CZP and a separate 3-mm-diam CS, which was mounted in close proximity to the CZP with thin copper wires. The CS had a 1-mm-diam pinhole in the center (“pinhole No. 1”). The focal length of the CZP at $\lambda=2.88\ \text{nm}$ is 77.44 mm and the distance between the source and the CZP was 167 mm. Using the +first diffraction order of the zone plate, the source was imaged by the CZP with a magnification of $0.9\times$ in the image plane 144 mm behind the CZP. The second pinhole (“pinhole No. 2”), having a diameter of 3 mm, was located in the image plane to select the x rays diffracted by the CZP in the first diffraction order as well as the x rays passing pinhole No. 1. Radiation diffracted in the 0th order and most of the radiation diffracted in other diffraction orders than the +first were blocked by pinhole No. 2. X rays passing pinhole No. 2 were detected by a charge coupled device (CCD) with 1024×1024 pixels at a distance of 730 mm behind the CZP. Figure 6 shows the defocused image of the source (+first diffraction order of the CZP) and a shadow image of the pinhole in the CS as recorded by the CCD. The number of counts within the shadow pinhole im-

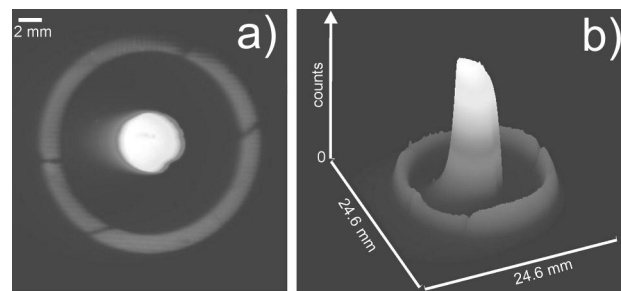


FIG. 6. (a) CCD image of the diffraction pattern. The ring corresponds to the signal of the first diffraction order of the CZP. The central peak corresponds to the x rays passing the pinhole in the central stop. (b) Three-dimensional surface plot of the left image.

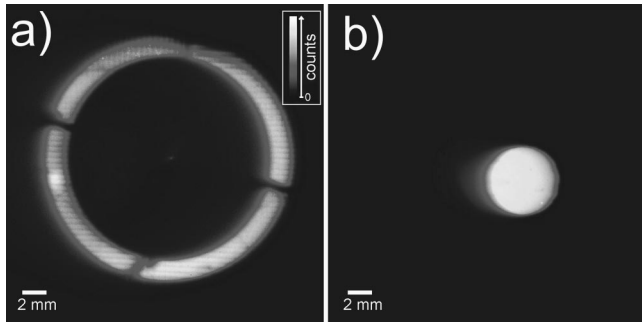


FIG. 7. (a) CCD image of the first diffraction order of the CZP. (b) Shadow image of a 1 mm diam pinhole.

age is proportional to the incoming x-ray intensity, reaching the CZP area. The number of counts within the defocused source image is proportional to the intensity diffracted by the CZP in the +first diffraction order. The efficiency was obtained from these two signals, by also taking the ratio between the pinhole area and the CZP area into account. Since both signals were attenuated by the absorption in the same Si_3N_4 support foil of the CZP, the groove efficiency of the CZP was measured, which is independent from the thickness of the CZP support foil.

An alternative but similar measurement method of the groove efficiency was performed as follows. First a CCD image was recorded by using a CS without a pinhole in the center [cf. Fig. 7(a)]. Then the CS was replaced by a 1 mm diam pinhole and a shadow image of the pinhole, attenuated by the absorption in the CZP support foil, was recorded [cf. Fig. 7(b)]. The efficiency is calculated from the ratio of the two images.

Since there is a simple geometric relation between a specific area in the CZP ring and the corresponding area in the defocused image (cf. Fig. 5), the CCD image also shows the relative local efficiency within the CZP pattern. For example, Fig. 7(a) indicates that the efficiency in the outer upper part of the CZP ring is lower compared to the rest of the CZP. This is in agreement with SEM images of the CZP where the nickel zones of the corresponding area of the CZP exhibit a strong deviation from the ideal line-to-space ratio, leading to a lower efficiency. The four narrow dark lines in the CCD image (cf. Fig. 7), which are subdividing the ring in four quarters, are caused by the shadow of the copper support wires for the central stop.

The groove efficiency of the CZP, as determined by the single-image method (Fig. 6), is 11.0 (± 2)%. The error of the efficiency measurement was estimated by taking the following two factors into account. A small error is due to an uncertainty in the geometric distances and the pinhole size. The major part of the error is due to a long, low intensity, tail of the x-ray source. This tail leads to a difficulty in separating the two signals (pinhole- and defocused source image).

The groove efficiency of the CZP, determined by the double image method (Fig. 7), is 11.7 (± 3.4)%. The error is due to an uncertainty in the geometric distances, and source intensity fluctuations between recording the two images. The

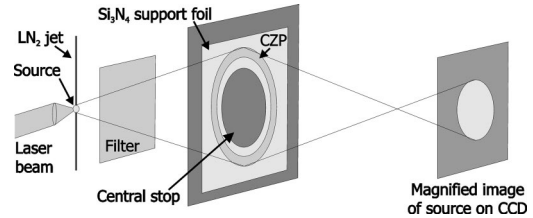


FIG. 8. Experimental arrangement for the source-size measurement.

last mentioned error was determined from statistical analysis of 20 images.

From the above we conclude that both methods are suited for measuring the efficiency and that the groove efficiency of the CZP in +first diffraction order at $\lambda = 2.88$ nm is 11%. For comparison, the calculated theoretical value (assuming 200 nm high nickel zones, a line-to-space ratio of 1:1, and a rectangular zone profile) for the efficiency at 2.88 nm wavelength is 20.9%.⁹ However, by using the CZP in the x-ray microscope, the absolute efficiency at $\lambda = 2.478$ nm is of interest. This can be calculated from the measured groove efficiency by taking the slightly different wavelength into account and the absorption of the support foil. The support foil consists of a 150 nm thick Si_3N_4 foil with deposited layers of 5 nm Cr and 10 nm Ge, resulting in 46% transmission at 2.478 nm. Therefore an absolute efficiency of 5.5% at $\lambda = 2.478$ nm is expected. The theoretical value for the absolute efficiency at $\lambda = 2.478$ nm is 10.0%.

IV. IMAGING PROPERTIES OF THE CZP

In order to verify the expected CZP imaging properties discussed in Sec. II, the laser-plasma source was imaged by the CZP in +first diffraction order as shown in Fig. 8. The source size at $\lambda = 2.88$ and 2.478 nm was measured. For generating the plasma a Nd:ytrium-aluminum-garnet laser generating 3 ns long pulses with typically 90 mJ/pulse ($\lambda = 532$ nm) was used. To suppress scattered green laser light a filter (600 nm Ti for measurements at $\lambda = 2.88$ and 200 nm Zr for $\lambda = 2.478$ nm) was placed between the source and the CZP. A 3 mm diam copper disk was mounted behind the CZP as a CS. The magnified image of the source was recorded by a CCD.

For the measurements at $\lambda = 2.88$ nm, a magnification of 25 \times was chosen (distance CZP-CCD 2030 mm, focal length of CZP at 2.88 nm is 77.44 mm). At this magnification a 24 μm wide CCD pixel corresponds to 0.96 μm in the source plane. For imaging the source at $\lambda = 2.478$ nm, the magnification was 21 \times , (distance CZP-CCD 2015 mm, focal length of CZP at 2.478 nm is 90.0 mm). Figure 9 shows the image of the source at $\lambda = 2.478$ nm. The measured FWHM of the source in the direction of the laser beam focused on the LN_2 jet is $x = 20$ μm and perpendicular to this direction, $y = 19$ μm . For $\lambda = 2.88$ nm, we found $x = 17$ μm and $y = 18$ μm . These values are in good agreement with previous measurements of the source size^{12,14} using a zone plate fabricated by holographic methods.⁵ Thus, the imaging properties of the fabricated CZP are in line with expectations and

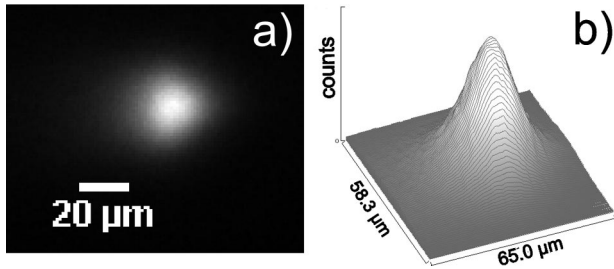


FIG. 9. Liquid N_2 jet laser-plasma source-size measurement with the CZP at $\lambda=2.478$ nm: (a) CCD image and (b) three-dimensional plot of the CCD signal.

the broadening of the spot due to the stitched fields and field misplacement due to drift is small on the scale of the $20 \mu\text{m}$ source (cf. Sec. II). It may therefore be concluded that the fabricated CZP has proper imaging properties for the compact x-ray microscope. Furthermore, it can also be used for plasma-source diagnostics.

V. CONCLUSIONS

A CZP with 49 nm outermost linewidth and a diameter of 4.53 mm was fabricated. It is shown that the significant misplacement of the single write fields during the e-beam exposure has a negligible influence of the required imaging properties of the CZP for the object illumination purpose in a compact x-ray microscope. Furthermore, we have demonstrated a concept for measuring the groove efficiency using a laser-plasma source. The fabricated CZP is found to have a groove efficiency of $11\% \pm 2\%$ at $\lambda=2.88$ nm in the +first diffraction order. The measurement allows us to carry out the characterization of these devices in-house. Additionally we did a source size measurement of the plasma source using the CZP. The results are in agreement with previous measure-

ments and demonstrate that the CZP will also be a useful tool for plasma source characterizations. A calibration of the CCD camera and a transmission measurement of the Si_3N_4 support foil will allow us to measure absolute spectral brightness values of the source in the future.

ACKNOWLEDGMENTS

The authors gratefully acknowledge the valuable discussion with G. Schneider and T. Wilhein. They also like to thank A. Liljeborg for lab support. This work was supported by the Swedish Science Research Council.

- ¹G. Schmahl, D. Rudolph, B. Niemann, P. Guttman, J. Thieme, G. Schneider, M. Diehl, and T. Wilhein, *Optik (Jena)* **93**, 66 (1993); J. Kirz, C. Jacobsen, and M. Howells, *Q. Rev. Biophys.* **28**, 33 (1995).
- ²M. Berglund, L. Rymell, M. Peuker, T. Wilhein, and H. M. Hertz, *J. Microsc.* **197**, 268 (2000); G. A. Johansson, A. Holmberg, H. M. Hertz, and M. Berglund, *Rev. Sci. Instrum.* **73**, 1193 (2002).
- ³M. Berglund, L. Rymell, T. Wilhein, and H. M. Hertz, *Rev. Sci. Instrum.* **69**, 2361 (1998).
- ⁴F. Eriksson *et al.* (unpublished).
- ⁵M. Hettwer and D. Rudolph, in *X-ray Microscopy and Spectromicroscopy*, edited by J. Thieme, G. Schmahl, D. Rudolph, and E. Umbach (Springer, Heidelberg, 1998), Chap. IV-27.
- ⁶T. Schliebe, *Microelectron. Eng.* **41/42**, 465 (1998).
- ⁷E. H. Anderson, D. L. Olynick, B. Harteneck, E. Veklerov, G. Denbeaux, W. Chao, A. Lucero, L. Johnson, and D. Attwood, *J. Vac. Sci. Technol. B* **18**, 2970 (2000).
- ⁸G. Schmahl and D. Rudolph, *Optik (Jena)* **29**, 577 (1969); B. Niemann, D. Rudolph, and G. Schmahl, *Opt. Commun.* **12**, 160 (1974).
- ⁹J. Kirz, *Opt. Commun.* **64**, 301 (1974).
- ¹⁰A. Holmberg, S. Rehbein, and H. M. Hertz, *Microelectron. Eng.* (in press).
- ¹¹M. Born and E. Wolf, *Principles of Optics*, 7th ed. (Cambridge University Press, Cambridge, UK, 1999).
- ¹²U. Vogt, R. Frueke, T. Wilhein, H. Stollberg, P. A. C. Jansson, and H. M. Hertz, *Appl. Phys. B: Lasers Opt.* **78**, 53 (2004).
- ¹³www-cxro.lbl.gov
- ¹⁴P. A. C. Jansson (personal communication).